Broadband high-contrast visible optical switches based on a spin-crossover material

Stéphane Calvez, Henri Camon, Karl Ridier, Gábor Molnár, Olivier Gauthier-Lafaye

Published in *Applied Optics*, **61**, 9562-9568 (2022) -- doi: 10.1364/AO.473176

Broadband high-contrast visible optical switches based on a spin-crossover material

STEPHANE CALVEZ,[1,*] HENRI CAMON, [1] KARL RIDIER,[2] GABOR MOLNAR,[2] AND OLIVIER GAUTHIER-LAFAYE[1]

[1]LAAS-CNRS, Université de Toulouse, CNRS, 7 avenue du colonel Roche, F-31400 Toulouse, France
[2]LCC-CNRS, Université de Toulouse, CNRS, 205 Route de Narbonne, F-31077 Toulouse, France
**scalvez@laas.fr*

Abstract: Visible optical switches embedding a spin-crossover thin film and exploiting frustrated total internal reflection operation principle are studied and optimized numerically with a view to obtain broadband high-contrast devices. A practical implementation using uncoated SF11 prisms embedding a 1-µm-thick layer of iron-triazolyl-borate complex as the thermo-active phase-change material is shown to support p-polarized modulation with a contrast in excess of 90% over a spectral bandwidth greater than 270 nm and over an angular acceptance bandwidth of 0.45°, surpassing the performance achievable with optically-resonant devices.

1. Introduction

Active optical devices capitalizing upon the large variation of the complex refractive index associated with the externally-activated electronic and/or structural phase transition of optical Phase-Change Materials (PCMs) have received a lot attention over the last two decades. Indeed, these materials provide index variations that are orders of magnitude higher than electro-optic or carrier-induced effects which means that they can introduce tunability or reconfigurability with a much smaller thickness of material, and that they consequently offer tantalizing prospects of improved optical components including smart windows [1,2], optical memories [3], spatial light modulators [4,5] or even (neuromorphic) photonic integrated circuits [6,7]. In all these cases, given the central role played by the embedded PCM, its selection is based on the targeted use and on the device operating wavelength range. In practice, the PCM absorption properties have meant that (near) infrared devices predominantly make use of chalcogenides (e.g. $Ge_2Sb_2Te_5$) or transition metal oxides (e.g. vanadium oxides V_xO_y), while visible devices have relied on liquid crystals.

To alleviate some of the drawbacks of liquid crystals which include polarization-dependent, low-frequency (sub-MHz) response and the need for hermetically-sealed packaging to deal with their liquid phase, we have recently proposed to use all-solid spin-crossover (SCO) complexes. Indeed, these thermally responsive molecular compounds, which can switch reversibly between their low-spin (LS) and high-spin (HS) electronic configurations, exhibit a drastic change of their optical properties upon the spin transition [8,9]. In particular, their prime representative of formula $[Fe(HB(1,2,4\text{-triazol-1-yl})_3)_2]$ displays abrupt hysteresis-free transitions between the low and high spin states at temperatures (65°C) close to room temperature that are accompanied by an absorption-free refractive index modulation of 0.07 in the visible [10,11] with tens of megahertz modulation speed capabilities [12]. Furthermore, metallic-mirror Fabry-Pérot interferometers [11] embedding an evaporated thin film of the above-mentioned complex have enabled the demonstration of resonant visible-light switches whose modulation depth was however limited to less than 40% and whose spectral bandwidth was also lower than a few nanometers.

Published in *Applied Optics*, **61**, 9562-9568 (2022) -- doi: 10.1364/AO.473176

In this paper, we numerically evaluate and optimize the response of different switches embedding a thin film of the same spin-crossover compound and exploiting Total Internal Reflection (TIR) to design experimentally-viable broadband high-contrast switches.

2. Device geometry and operating principle considerations

The geometry of the switch under study is shown in Fig. 1 and was first introduced by Kashnow et al [13] to implement a liquid-crystal-based modulator. It consists in a layer of the SCO material of refractive index, n_{SCO}, inserted between two prisms of higher refractive index, n_p, to enable TIR at the prism/SCO interface for internal incident angles, θ_p, greater than the TIR limit angle, $\theta_{p,TIR}$, given by:

$$\theta_{p,TIR} = asin\left(\frac{n_{SCO}}{n_p}\right) \quad (1)$$

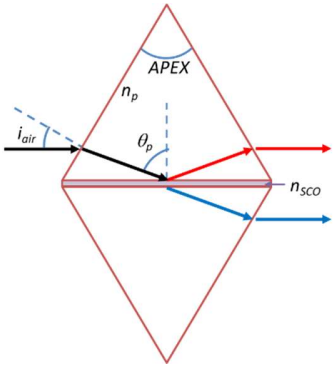

Fig. 1. Diagram of the double-prism Total-Internal-Reflection SCO-based switches under study.

Should the SCO region be a bulk anti-reflection-coated half-cylinder or half-sphere [14,15], the principle of operation of this switch can be readily explained from the above consideration alone. As the temperature of the assembly (and of the SCO material in particular) rises, the SCO material transits from its Low-Spin (LS) state to High-Spin (HS) state, and its refractive index switches from a high to a low value (specifically, at the green wavelength of λ=532 nm, from $n_{SCO,LT}$(532 nm)=1.618 to $n_{SCO,HT}$(532 nm)=1.566), decreasing accordingly the TIR limit angle from, $\theta_{p,TIR,LT}$ to $\theta_{p,TIR,HT}$ (see Eq. 1 where the temperature change of the prism refractive index is neglected as it is more than one order of magnitude smaller than the one of the SCO). Should the impinging visible light be incident at an angle, θ_p, chosen to be comprised between these two boundaries, the light will switch from being transmitted at low temperatures to being reflected at high temperatures, resulting in a nominally high-contrast modulation. Furthermore, given that the underlying effect is free of any (optical) resonance and that only transparent (weakly-dispersive) materials are involved, the modulation is also due to be spectrally broadband. It is nevertheless interesting to point out as an insight into the device behavior that, since $\theta_p \leq \theta_{p,TIR,LT}$, the light propagation into the SCO medium at low temperatures has to occur at an angle larger than $asin(n_{SCO,HT}/n_{SCO,LT})$=75.4° i.e. fairly close to the prism interfaces..

The operating principle of the device is however somewhat modified by the fact that the SCO material is a thin film. Indeed, the second (outer) SCO/prism interface creates a Fabry-Pérot interferometer excited under oblique incidence, setting the overall device characteristics. It is however worth noting, as an insight into the resulting behavior, that the nominally TIR reflection at high temperatures ($\theta_p > \theta_{p,TIR,HT}$) will be compromised by optical tunneling [16] through the SCO layer as soon as the second (outer) SCO/prism interface is positioned within the TIR penetration length which is controlled by θ_p and given by :

Published in *Applied Optics*, **61**, 9562-9568 (2022) -- doi: 10.1364/AO.473176

$$L_{pen} = \frac{\lambda}{4\pi\sqrt{n_p^2 sin^2(\theta_p) - n_{SCO,HT}^2}} \quad (2)$$

As a preliminary step in the design of the device, the evolution of the two TIR angles as a function of the refractive index of the embedding prisms is represented in Fig. 2. It can clearly be seen that both the mean value and the angular difference decrease with increasing prism refractive index. The latter observation suggests that there is a compromise between using low index prisms to achieve high angular tolerance and using high index prisms to avoid operation at grazing incidence. The lower part of Fig. 2 illustrates that the TIR penetration depth into the SCO dependence on the in-prism incidence angle, θ_p, and indicates an intrinsic minimum value, achieved for θ_p=$\theta_{p,TIR,LT}$, of $\lambda/\left(4\pi\left(n_{SCO,LT}^2 - n_{SCO,HT}^2\right)^{0.5}\right)$~102 nm.

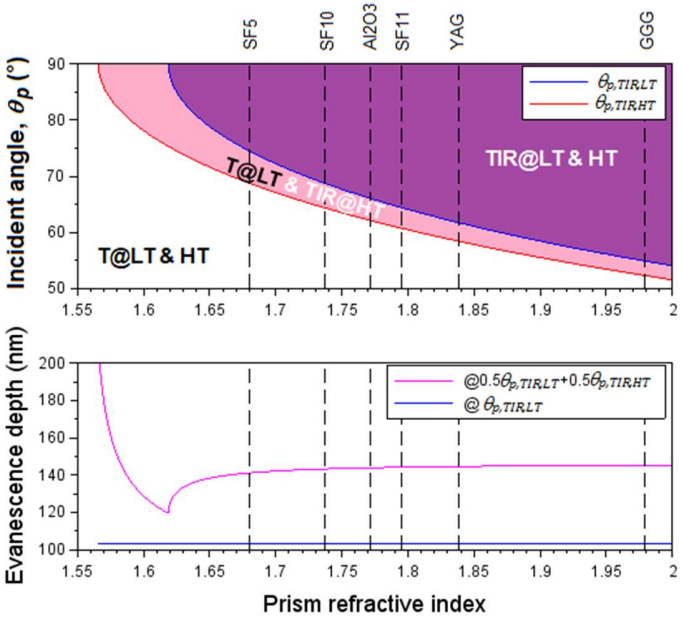

Fig. 2. Prism refractive index dependence of the TIR characteristics (at a wavelength of 532 nm) at the prism/SCO interface. The vertical dash lines indicate the refractive index of relevant prism materials.

3. Results and discussion

3.1 Fixed wavelength operation

The numerically studied device is a thermo-activated switch based on the SCO complex [Fe(HB(1,2,4-triazol-1-yl)$_3$)$_2$] reported in [11] which exhibits an relatively abrupt and complete transition when applying a 10°C variation around 65°C. Given that this compound is highly transparent in the visible region, the system reflection and transmission exit paths (in red and blue respectively on Fig. 1) are complementary one another. The performance of the switch will therefore only be presented in term of the modulation contrast induced by spin-state switching. This parameter is thus taken to be the difference in the system reflection triggered by varying the SCO temperature between 25 and 80°C. This figure-of-merit (FoM=R_{HT}-R_{LT}) is calculated using the generalized transfer matrix method [17] using the reported dispersion relations of the SCO layer [11] and of the various prism materials considered (Schott SF5, SF10, and SF11 glasses [18] and crystals of synthetic sapphire [19], yttrium aluminum garnet (YAG) [20] and gadolinium gallium garnet (GGG) [21]) and taking into account that the SCO thickness expands by 4.7% upon its phase transition.

Published in *Applied Optics*, **61**, 9562-9568 (2022) -- doi: 10.1364/AO.473176

SF11 prisms being commonly available since they are used as dispersion compensation elements in ultrafast lasers [22], the study begins by investigating the response of a configuration with SF11 prisms. First, the angular dependence of the switch reflectivity curves and associated reflection contrasts at the design wavelength of 532 nm for set SCO thicknesses of 100 and 700 nm is presented on Fig. 3 for both TE- and TM-polarized light. The evolution of the reflection contrasts for SCO thicknesses up to 1 µm are then shown as an extension on Fig. 4.

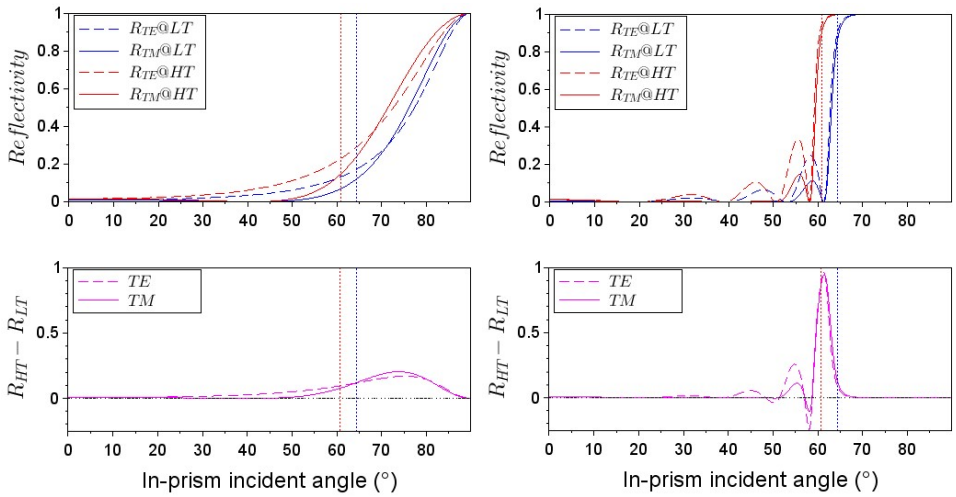

Fig. 3. Angular dependence of a SF11-prism switch reflection and reflection contrast at a wavelength of 532 nm for TE and TM-polarized light and an SCO thickness of (left) 100 nm and (right) 700 nm. The vertical dotted blue (resp. red) line represents the TIR angle for the SCO in its low-spin state i.e held at low temperature (LT) (resp. high-spin state and high temperature (HT)).

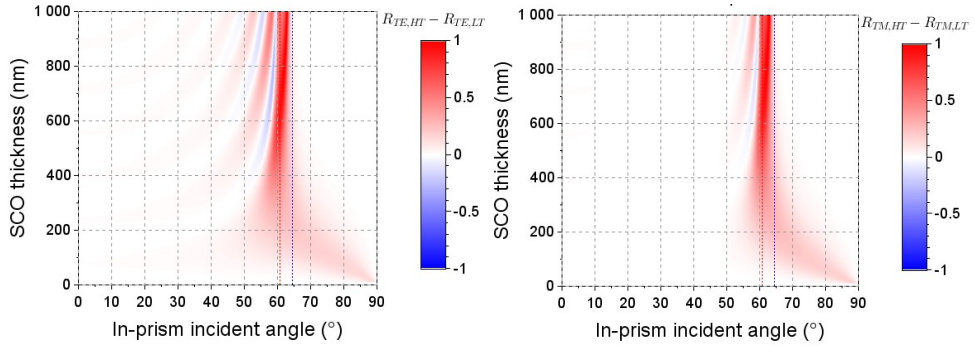

Fig. 4. Angular dependence of a SF11-prism switch reflection contrast at a wavelength of 532 nm as a function of SCO thickness for (left) TE-polarized light and (right) TM-polarized light. The vertical dotted blue (resp. red) line represents the TIR angle for the SCO in its low-spin state i.e held at low temperature (LT) (resp. high-spin state and high temperature (HT)).

For both polarizations and (<~300-nm) thin SCO layers, the device reflection increases with temperature and the reflectivity contrast is observed to reach its maximum at a prism internal incidence angle that is seen to decrease linearly with SCO thickness but is also systematically larger than the critical angles ($\theta_{p,TIR,LT}$=64.4° and $\theta_{p,TIR,HT}$=60.7°). As indicated in section 2, this behavior stems from the fact that, for these thin layers, optical tunneling occurs. The reflection is therefore far from being total even above the TIR angles which, in turn, translates into a limited modulation depth. For thicker SCO layers and as illustrated on the right part of Fig. 3,

Published in *Applied Optics*, **61**, 9562-9568 (2022) -- doi: 10.1364/AO.473176

the reflectivity curves exhibit steep reflectivity variations around the critical angles and damped-oscillatory patterns at smaller incident angles. The pseudo-periodicity of these oscillations increases with the SCO thickness, a fact consistent with the appearance of higher-order longitudinal modes in the Fabry-Pérot interferometer established by the two SCO/prism interfaces. In the TM-polarized case, a stronger damping is observed for angles below 50° as a result of the much reduced reflectivity of the SCO/prism interfaces around the Brewster angle (~41°). The angle for which the maximum reflectivity difference is achieved is observed to be bound by the critical angles. This maximum-modulation-depth angle, $\theta_{p,opt}$, is also seen to slightly increase with SCO thickness as a result of a compromise. Indeed, at high temperature, this optimum angle should be much higher than $\theta_{p,TIR,HT}$ (i.e. have a small penetration depth) to limit the leakage into the SCO material and potential transmission through the whole assembly. On the contrary, at low temperature, it should be much lower than $\theta_{p,TIR,LT}$ so that the angle of propagation in the SCO material is as small as possible thereby limiting the interaction path along the interfaces and reducing the device size. It is worth pointing out that, for a 1-µm-thick SCO layer, the TM-polarized (respectively TE-polarized) modulation depth exceeds 90% over a full bandwidth of 0.45° (resp. 0.65°) and reaches a maximal value greater than 99.9 % (resp. 99.8%) at the optimal illumination in-prism angle, $\theta_{p,opt}$, of 62.825° (resp. 62.825°).

A similar behavior is obtained for devices using other materials than SF11 for the two prisms. Indeed, as evidenced on Fig. 5, the maximal (TM-polarized) modulation depth follows an S-shape dependence on SCO thickness while the corresponding optimal excitation angle decreases rapidly from glazing incidences to be within TIR bounds (pink region on Fig. 2) and before slowly and asymptotically increasing towards $\theta_{p,TIR,HT}$. It is worth highlighting that, for thin SCO layers, the maximum modulation depth increases as the prism refractive index gets closer to the SCO values, and that, for SCO thicknesses greater than 700 nm and independently of the chosen prism material, the obtained reflection contrast values are in excess of 93%. Additionally, the SCO layer thickness required for the optimum angle to stabilize within the TIR bounds (i.e. between $\theta_{p,TIR,LT}$ and $\theta_{p,TIR,HT}$) and, equivalently, for achieving high contrast switching is observed to decrease as the prism refractive index increases (from 250 nm for SF5 to 179 nm for GGG). However, this (marginal) improvement afforded by using high index prisms comes at the expense of a reduced angular acceptance bandwidth (see Table 1). The latter both properties actually directly stem from Eq. (1) and (2) or from Fig. 2.

Published in *Applied Optics*, **61**, 9562-9568 (2022) -- doi: 10.1364/AO.473176

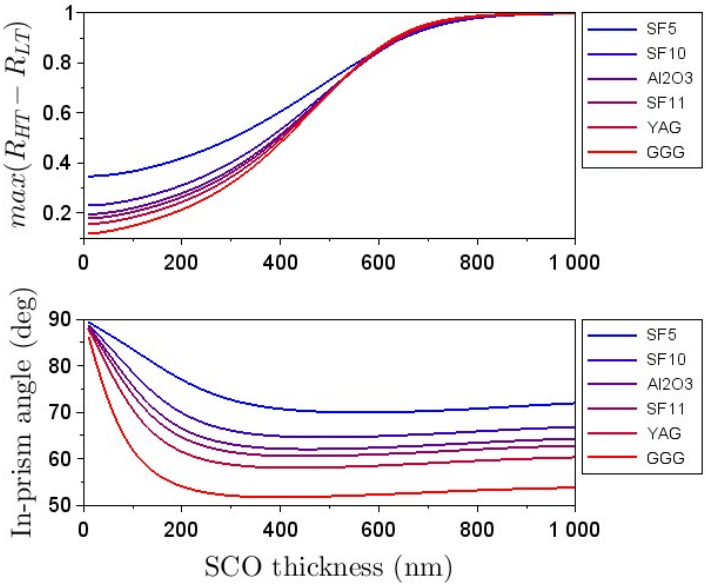

Fig. 5. SCO-thickness evolutions of the maximum reflection contrast and of the corresponding in-prism optimum excitation angle under TM-polarized 532-nm-wavelength illumination. The prism materials are listed by increasing order of refractive index (the latter being always greater than the SCO values – see Fig. 2)

Up to this point, we have considered the device to be perfect. In practice, the SCO layer will be deposited either simultaneously on the two prisms which will be pressed one against the other forming a symmetric mounting configuration, or the evaporation will be carried out on one prism only in which case the mounting will be asymmetric (see inset of Fig. 6 left). In both cases, an air gap may however arise as a result of an imperfect assembly (typically due to a mismatch in the planarity of the prisms). As shown on the left of Fig. 6, the prime consequence of the presence of a planar air gap is an undesirable yet drastic reduction in the achievable modulation depth, irrespective of the selected mounting strategy. In practice, the two pressed surfaces will be in partial contact and a refined estimate of the performance deterioration (under incoherent illumination) can be obtained as the spatial average of the response of Fig.6 over the optical beam.

Published in *Applied Optics*, **61**, 9562-9568 (2022) -- doi: 10.1364/AO.473176

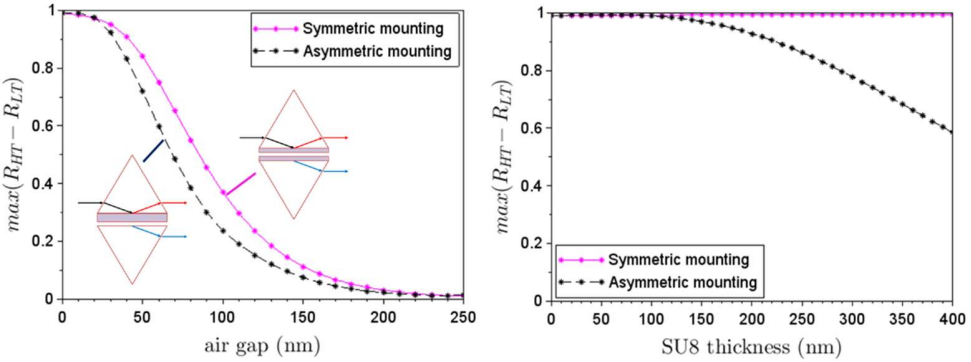

Fig. 6. Influence of (left) an air gap and (right) an SU8 layer (of refractive index of 1.585) on the performance of a SF11 prism setup and a SCO layer of total thickness of 800 nm with schematics of the two considered mounting configurations. Calculations performed for 532-nm-wavelength TM-polarized illumination.

To avoid the latter artefact, two approaches could considered; the most straightforward approach being to cement the assembly using an appropriate optical glue while the alternative solution would exploit prisms with convex large-curvature contact faces [23]. As can be observed on the right of Fig. 6, using cured SU8 photoresist as the glue (which may be applied by spin coating or inkjet printing and whose refractive index is taken to be 1.585) high-contrast modulation can be maintained for glue thicknesses lower than 400 nm when using the symmetric mounting.

3.2 Spectral performance

The calculations reported in the previous paragraph suggest that a SCO layer embedded between two higher index prisms is amenable to form a thermally-activated switch with high modulation depth should the layer be sufficiently thick and the in-prism angle be carefully selected. Hereafter, we investigate the resulting spectral characteristics of such a system.

It can be easily shown using geometrical considerations and Snell's law that the angle of incidence in air, i_{air}, on the prism can be related to the prism full apex angle, A, and the optimal in-prism angle, $\theta_{p,opt}$, using the following expression:

$$\sin(i_{air}) = n_p \cdot \sin(\pi/2 - A/2 - \theta_{p,opt}) \quad (3)$$

As a result and as illustrated on the Fig. 7 left, the incidence angle (in air) at the design wavelength can be adjusted by tuning the prism apex angle (and vice versa). Varying this parameter also leads to a modification of the signal transmission through the (uncoated-prism) in/out-coupling interfaces and to the change of the in-prism angular dispersion characteristics (see Fig. 7 right), both which affect the overall device spectral performance.

Published in *Applied Optics*, **61**, 9562-9568 (2022) -- doi: 10.1364/AO.473176

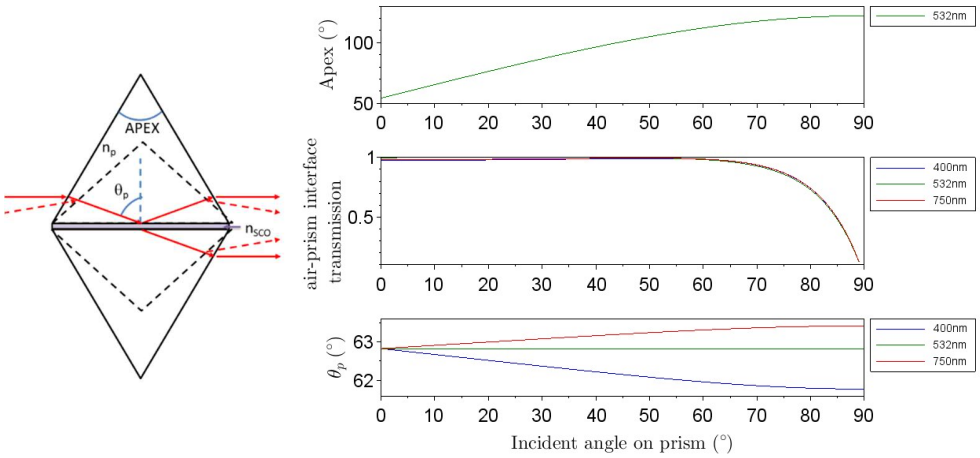

Fig. 7. Left, Illustration of the relationship between the prism apex angle and the system beam propagation paths and, right, resulting modifications of the in/output beam characteristics for an SF11 prism system designed for TM-polarized operation at 532 nm.

Taking all these effects into account leads to the spectral map of Fig. 8 for a SF11 prism device. Although not directly shown here, analyzing the effects separately reveals that the angular dispersion leads to a monotonous improvement in the 90%-depth modulation bandwidth as the incidence angle increases (the bandwidth short wavelength limit decreasing from 450 down to 426 nm as noticeable from the evolution of the drawn (visible-wavelength) 90%-depth contour of Fig. 8). Besides, as expected and observable from the angular bounds of the 90%-depth contour of Fig. 8, the degradation of the transmission of the uncoated interfaces (see Fig. 7. right) compromises the performance at low incidence angles and even more substantially at high incidence angles, leading to an operational sweet spot around Brewster's angle.

Published in *Applied Optics*, **61**, 9562-9568 (2022) -- doi: 10.1364/AO.473176

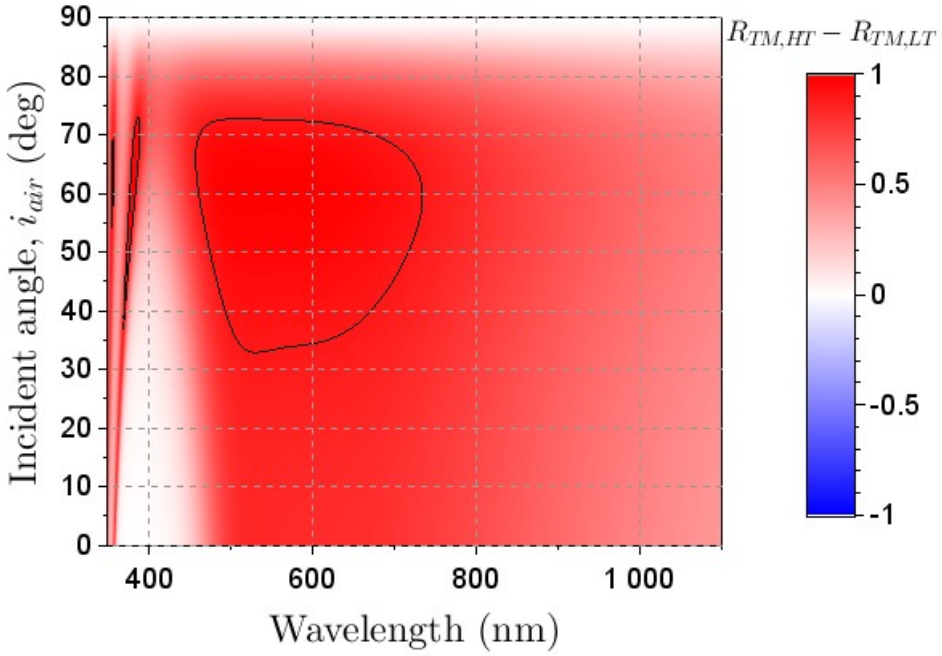

Fig. 8. Spectral characteristics of an SF11-prism-based device embedding a 1µm-thick SCO layer as a function of the light incidence angle, i_{air}, (or equivalently of the prism apex – see Fig. 7 or Eq. (3)) – The black lines highlight the 90% switching contrast limits.

For sake of completeness, the calculated modulation spectra that can be achieved with a 1µm-thick SCO layer and prisms made of either of the 6 considered materials are presented in Fig. 9. The relevant characteristic parameters are summarized in Table 1. The glass-based prisms allow spectrally broader modulation than the crystalline ones. The configuration with the highest potential, i.e. having the broadest angular and spectral bandwidths, turns out to be the one based on SF5. A switch using SF11 prisms might however be preferred given the more widespread availability of prisms made of this material but this choice will come at the expense of a penalty in the foreseeable performance.

Published in *Applied Optics*, **61**, 9562-9568 (2022) -- doi: 10.1364/AO.473176

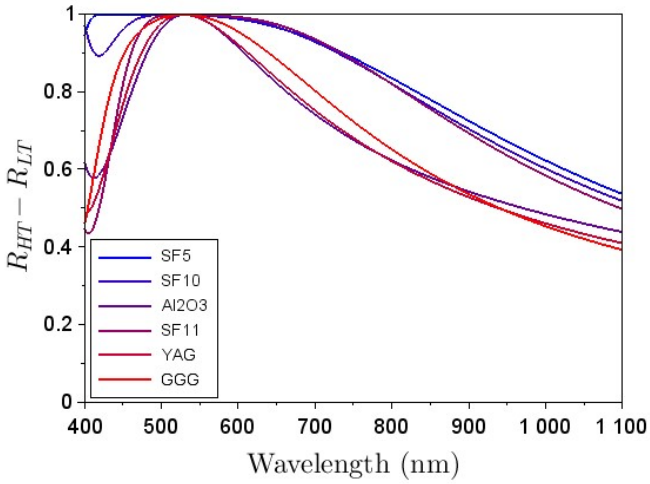

Fig. 9. Spectral characteristics of devices embedding a 1µm-thick SCO layer and operated in TM-polarization at Brewster's angle of incidence on the prisms.

Table 1. Main characteristics of TIR switches embedding a 1µm-thick SCO layer between two prisms. The devices are assumed to be operated under TM-polarized excitation

Prism Material	n_p(532nm)	$\theta_{p,opt}$ (°) @e_{SCO}=1µm	$\Delta\theta_{p,opt}$ (°)	Apex (°) for $i_{air}=i_{Brewster}$	λ_{min} (nm) for R_{HT}- R_{LT}>90%	λ_{max} (nm) for R_{HT}- R_{LT}>90%	$\Delta\lambda$ (nm) with R_{HT}- R_{LT}>90%
SF5	1.6796	71.95	1.55	97.6	401	735	334
SF10	1.7367	66.85	0.725	106.1	426	727	301
Sapphire	1.771	64.32	0.525	110.2	482	607	125
SF11	1.7948	62.825	0.45	112.6	460	733	273
YAG	1.838	60.32	0.35	116.5	475	612	137
GGG	1.978	53.8	0.2	126.0	452	639	187

4. Conclusions

A numerical investigation of visible optical switches constituted of a sub-micrometer-thick spin-crossover thin film surrounded by two higher-index prisms and exploiting total internal reflection has been carried out to evaluate the potential of this approach to surpass the performance achievable with optically-resonant devices.

The study has shown that this configuration, originally used with liquid-crystal modulator cell, is amenable to sustain high-contrast modulation with ~1° angular acceptance and a spectral bandwidth exceeding the visible range in spite of the reduced switching layer thickness. Although the calculations were performed with the particular material switching characteristics of the complex of formula $[Fe(HB(1,2,4\text{-triazol-1-yl})_3)_2]$, the similarity in the refractive index of spin-crossover materials suggest that the results are broadly applicable to devices embedding

other transition-metal complexes. This work will be followed by practical experimental demonstrations of this type of thermally-driven switches in light of the expected promising modulation performance. The latter investigations will certainly be carried out in two steps starting with establishing the proof-of-concept where the full assembly will be heated/cooled and subsequently working on improving the switching dynamics using refined embodiments which are likely to exploit prisms of small dimensions and (UV-light)-photo-induced localized heating.

Funding. CNRS MITI project "CMTS-SLM" and Université Paul Sabatier TREMPLIN grant "MaCaPeSuMO".

Disclosures. The authors declare no conflicts of interest.

Data availability. Data underlying the results presented in this paper are not publicly available at this time but may be obtained from the authors upon reasonable request.

References

1. Y. Che, X. Wang, Q. Song, Y. Zhu, and S. Xiao, "Tunable optical metasurfaces enabled by multiple modulation mechanisms," Nanophotonics **9**, 4407–4431 (2020).
2. B. Ko, T. Badloe, and J. Rho, "Vanadium Dioxide for Dynamically Tunable Photonics," ChemNanoMat **7**, 713–727 (2021).
3. M. Wuttig, H. Bhaskaran, and T. Taubner, "Phase-change materials for non-volatile photonic applications," Nature Photon **11**, 465–476 (2017).
4. J. Beeckman, "Liquid-crystal photonic applications," Opt. Eng **50**, 081202 (2011).
5. Q. Wang, E. T. F. Rogers, B. Gholipour, C.-M. Wang, G. Yuan, J. Teng, and N. I. Zheludev, "Optically reconfigurable metasurfaces and photonic devices based on phase change materials," Nature Photon **10**, 60–65 (2016).
6. K. J. Miller, R. F. Haglund, and S. M. Weiss, "Optical phase change materials in integrated silicon photonic devices: review," Opt. Mater. Express **8**, 2415 (2018).
7. F. Brückerhoff-Plückelmann, J. Feldmann, C. D. Wright, H. Bhaskaran, and W. H. P. Pernice, "Chalcogenide phase-change devices for neuromorphic photonic computing," Journal of Applied Physics **129**, 151103 (2021).
8. G. Molnár, S. Rat, L. Salmon, W. Nicolazzi, and A. Bousseksou, "Spin Crossover Nanomaterials: From Fundamental Concepts to Devices," Adv. Mater. **30**, 1703862 (2018).
9. K. Abdul-Kader, M. Lopes, C. Bartual-Murgui, O. Kraieva, E. M. Hernández, L. Salmon, W. Nicolazzi, F. Carcenac, C. Thibault, G. Molnár, and A. Bousseksou, "Synergistic switching of plasmonic resonances and molecular spin states," Nanoscale **5**, 5288 (2013).
10. V. Shalabaeva, S. Rat, M. D. Manrique-Juarez, A.-C. Bas, L. Vendier, L. Salmon, G. Molnár, and A. Bousseksou, "Vacuum deposition of high-quality thin films displaying spin transition near room temperature," J. Mater. Chem. C **5**, 4419–4425 (2017).
11. Y. Zhang, K. Ridier, V. Shalabaeva, I. Séguy, S. Pelloquin, H. Camon, S. Calvez, L. Routaboul, L. Salmon, G. Molnár, and A. Bousseksou, "A molecular spin-crossover film allows for wavelength tuning of the resonance of a Fabry–Perot cavity," J. Mater. Chem. C **8**, 8007–8011 (2020).
12. K. Ridier, A. Bas, V. Shalabaeva, W. Nicolazzi, L. Salmon, G. Molnár, A. Bousseksou, M. Lorenc, R. Bertoni, E. Collet, and H. Cailleau, "Finite Size Effects on the Switching Dynamics of Spin-Crossover Thin Films Photoexcited by a Femtosecond Laser Pulse," Adv. Mater. **31**, 1901361 (2019).
13. R. A. Kashnow and C. R. Stein, "Total-Reflection Liquid-Crystal Electrooptic Device," Appl. Opt. **12**, 2309 (1973).
14. J. Fahrenfort, "Attenuated total reflection," Spectrochimica Acta **17**, 698–709 (1961).
15. T. R. Harrison, K. G. Scheuer, and R. G. DeCorby, "Tunable bandpass imaging filter based on resonant tunneling through a ball lens assembly," Appl. Opt. **59**, 7037 (2020).
16. P. W. Baumeister, "Optical Tunneling and Its Applications to Optical Filters," Appl. Opt. **6**, 897 (1967).
17. C. C. Katsidis and D. I. Siapkas, "General transfer-matrix method for optical multilayer systems with coherent, partially coherent, and incoherent interference," Appl. Opt. **41**, 3978 (2002).
18. Schott, "Optical glass data sheets," https://www.schott.com/en-gb/products/optical-glass-p1000267/downloads (September 2021).
19. I. H. Malitson, "Refraction and Dispersion of Synthetic Sapphire," J. Opt. Soc. Am. **52**, 1377 (1962).
20. D. E. Zelmon, D. L. Small, and R. Page, "Refractive-index measurements of undoped yttrium aluminum garnet from 0.4 to 5.0 μm," Appl. Opt. **37**, 4933 (1998).
21. D. L. Wood and K. Nassau, "Optical properties of gadolinium gallium garnet," Appl. Opt. **29**, 3704 (1990).
22. U. Keller, W. H. Knox, and H. Roskos, "Coupled-cavity resonant passive mode-locked Ti:sapphire laser," Opt. Lett. **15**, 1377 (1990).
23. Y. You, X. Wang, S. Wang, Y. Pan, and J. Zhou, "A new method to demonstrate frustrated total internal reflection in the visible band," American Journal of Physics **76**, 224–228 (2008).